Biochimica et Biophysica Acta 1807 (2011) 216–226

Contents lists available at ScienceDirect

Biochimica et Biophysica Acta

journal homepage: www.elsevier.com/locate/bbabio

Effects of formate binding on the quinone–iron electron acceptor complex of photosystem II

Arezki Sedoud [a], Lisa Kastner [a], Nicholas Cox [b], Sabah El-Alaoui [a], Diana Kirilovsky [a], A. William Rutherford [a,*]

[a] iBiTec-S, CNRS URA 2096, CEA Saclay, 91191 Gif-sur-Yvette, France
[b] MPI für Bioanorganische Chemie, Stiftstrasse 34-36/D-45470 Mülheim an der Ruhr, Germany

ARTICLE INFO

Article history:
Received 4 August 2010
Received in revised form 1 October 2010
Accepted 25 October 2010
Available online 29 October 2010

Keywords:
Photosystem II
Quinone
Non-heme iron
Formate
Bicarbonate
EPR

ABSTRACT

EPR was used to study the influence of formate on the electron acceptor side of photosystem II (PSII) from *Thermosynechococcus elongatus*. Two new EPR signals were found and characterized. The first is assigned to the semiquinone form of Q_B interacting magnetically with a high spin, non-heme-iron (Fe^{2+}, $S=2$) when the native bicarbonate/carbonate ligand is replaced by formate. This assignment is based on several experimental observations, the most important of which were: (i) its presence in the dark in a significant fraction of centers, and (ii) the period-of-two variations in the concentration expected for $Q_B^{\bullet-}$ when PSII underwent a series of single-electron turnovers. This signal is similar but not identical to the well-know formate-modified EPR signal observed for the $Q_A^{\bullet-}Fe^{2+}$ complex (W.F.J. Vermaas and A.W. Rutherford, FEBS Lett. 175 (1984) 243–248). The formate-modified signals from $Q_A^{\bullet-}Fe^{2+}$ and $Q_B^{\bullet-}Fe^{2+}$ are also similar to native semiquinone–iron signals ($Q_A^{\bullet-}Fe^{2+}/Q_B^{\bullet-}Fe^{2+}$) seen in purple bacterial reaction centers where a glutamate provides the carboxylate ligand to the iron. The second new signal was formed when $Q_A^{\bullet-}$ was generated in formate-inhibited PSII when the secondary acceptor was reduced by two electrons. While the signal is reminiscent of the formate-modified semiquinone–iron signals, it is broader and its main turning point has a major sub-peak at higher field. This new signal is attributed to the $Q_A^{\bullet-}Fe^{2+}$ with formate bound but which is perturbed when Q_B is fully reduced, most likely as Q_BH_2 (or possibly $Q_BH^{\bullet-}$ or $Q_B^{2\bullet-}$). Flash experiments on formate-inhibited PSII monitoring these new EPR signals indicate that the outcome of charge separation on the first two flashes is not greatly modified by formate. However on the third flash and subsequent flashes, the modified $Q_A^{\bullet-}Fe^{2+}Q_BH_2$ signal is trapped in the EPR experiment and there is a marked decrease in the quantum yield of formation of stable charge pairs. The main effect of formate then appears to be on Q_BH_2 exchange and this agrees with earlier studies using different methods.

1. Introduction

Photosystem II (PSII) is a chlorophyll-containing membrane-bound enzyme that uses the energy of light to take electrons from water and reduce plastoquinone (reviewed in [1,2]). The protein has two bound plastoquinones, Q_A and Q_B, which act as sequential electron acceptors. Although both are plastoquinones, their physical and chemical properties differ. Q_A is tightly bound and acts as a one-electron carrier while Q_B undergoes two sequential one-electron reduction steps. Q_B is weakly bound in its quinone and quinol form but tightly bound in its one-electron reduced semiquinone form (reviewed in [3]).

Excitation of the chlorophylls in PSII by light results in a charge separation forming a radical pair made up of a chlorophyll radical cation ($P_{680}^{\bullet+}$) and a pheophytin radical anion ($Ph^{\bullet-}$). The pheophytin radical anion subsequently reduces Q_A to $Q_A^{\bullet-}$. The $Q_A^{\bullet-}$ state is relatively short-lived (<1 ms) and undergoes no observable protonation events during its lifetime. $Q_A^{\bullet-}$ then reduces Q_B, forming $Q_B^{\bullet-}$, a tightly bound semiquinone that is thought to remain unprotonated. However, the negative charge is partially compensated by proton uptake by protein residues in close proximity to the semiquinone. After a second photochemical turnover, $Q_B^{\bullet-}$ undergoes a further one-electron reduction step. This event is coupled to protonation reactions forming Q_BH_2. Q_BH_2 leaves the Q_B site and is replaced by plastoquinone from the pool in the membrane, this gives rise to the characteristic two-electron gate phenomena associated with Q_B function [4–7].

The acceptor side electron and proton transfer reactions occurring in PSII are poorly understood compared to the related reactions occurring in the purple bacterial reaction center [8,9]. As a result the

Abbreviations: ANT2p, 2-(3-chloro-4-trifluoromethyl) aniline-3,5-dinitrothiophene; Cyt b_{559}, Cytochrome b_{559}; DAD, 2,3,5,6 tetramethyl-p-phenylenediamine; DCMU, 3-(3,4-dichlorophenyl)-1,1-dimethylurea; EPR, electron paramagnetic resonance; PSII, photosystem II; Q_A and Q_B, primary and secondary quinone electron acceptor of PSII

* Corresponding author. Tel.: +33 1 69 08 2940; fax: +33 1 69 08 87 17.
E-mail address: alfred.rutherford@cea.fr (A.W. Rutherford).

0005-2728/$ – see front matter © 2010 Elsevier B.V. All rights reserved.
doi:10.1016/j.bbabio.2010.10.019

working model for PSII is greatly influenced by insights from the purple bacterial reaction center [3]. The close structural similarity between the purple bacterial reaction center and PSII was indicated by the similar spectroscopic signatures from the semiquinone iron complex (reviewed in [10]). The crystallographic model from the purple bacterial reaction center [11] thus provided a good model for PSII [11,12], this was supported by amino acid sequence comparisons [13], mutagenesis [14,15], molecular modeling [16] and biochemistry [17,18]. The model was verified by extensive biophysical studies (e.g. [19,20]) and eventually by crystallography of PSII [21–23].

A high spin non-heme iron (Fe^{2+}, $S=2$) is located between the two bound quinones Q_A and Q_B. It is coordinated by four histidines, two from the D1 subunit (H215 and H272) and two from the D2 subunit (H214 and H268). In the bacterial reaction center, the fifth and sixth ligand to the iron is a bidentate carboxylate ligand from the glutamate M-E232 [11]. In PSII an exchangeable, bidentate bicarbonate/carbonate is the non-histidine ligand [10,11,24,25].

The depletion of bicarbonate/carbonate or its substitution by formate results in a slowing of the electron transfer rate from $Q_A^{\bullet-}$ to Q_B and to $Q_B^{\bullet-}$ by factors of five and ten, respectively [26–29]. The exchange of the Q_BH_2 with the plastoquinone pool is slowed down by more than a two orders of magnitude [27,30,31]. Some of these inhibitory effects maybe due to the perturbation and/or inhibition of the protonation reactions that are coupled to electron transfer [24]. A specific chemical model explaining how depletion of bicarbonate affects electron transfer in the quinone–iron complex has not yet been established (reviewed in [32,33]). Recent observations have suggested that carbonate rather than bicarbonate is the native ligand to the non-heme iron in PSII [34]. The additional negative charge on the carbonate ion compared to bicarbonate would be expected to be relevant to its purported roles in the proton-coupled electron transfer.

The existence of an exchangeable ligand on the iron that strongly affects the rate of electrons leaving PSII could reflect a regulatory mechanism of some kind. The natural ligand (CO_3^{2-}/HCO_3^-) is in equilibrium with CO_2, the terminal electron acceptor of photosynthesis. A role for CO_2 in regulating electron input into the electron transfer chain seems plausible. If however the slow down in electron transfer occurs simply upon protonation of carbonate (forming bicarbonate) [34], then the regulatory factor could be pH or the binding of another carboxylic acid.

The semiquinone radicals $Q_A^{\bullet-}$ and $Q_B^{\bullet-}$ in PSII and purple bacteria are magnetically coupled to the non-heme iron Fe^{2+} ($S=2$). This interaction strongly perturbs the radical signals as seen by EPR. Semiquinones generally appear as sharp structureless signals centered at $g\sim2.004$ but in PSII and purple bacterial reaction centers they interact with the Fe^{2+} leading to a broadening of their EPR lineshape. In PSII, the $Q_{A/B}^{\bullet-}Fe^{2+}$ complexes have turning points around $g\sim1.8$ and 1.9 [35–39], reviewed in [3,10]. The signal at $g=1.9$ is the native form [37] while the $g=1.8$ form is seen when formate or other carboxylic acids replace the bicarbonate/carbonate ion [38]. In PSII isolated from the cyanobacterium, *Thermosynechococcus elongatus*, the same phenomenology is observed [40,41]. The presence of the $g=1.8$ form in samples that have not been treated with a carboxylic acid [35–37] presumably reflects those (non-native) centers: (i) in which the (bi) carbonate ion is absent, or (ii) in which the native carbonate is replaced by bicarbonate (see [34]). In either case, the $g=1.8$ form probably represents non-functional centers [42]. The addition of formate to PSII significantly increased the amplitude of the $Q_A^{\bullet-}Fe^{2+}$ EPR signal by converting the weak $g=1.9$ signal to a well resolved $g=1.8$ signal [38]. This simple biochemical procedure is routinely employed to allow $Q_A^{\bullet-}Fe^{2+}$ to be monitored (e.g. [40,41]). Some other carboxylic acids have been shown to have smaller effects on the $Q_A^{\bullet-}Fe^{2+}$ in plant PSII showing competitive binding effects with the much more pronounced formate effect [43].

$Q_B^{\bullet-}Fe^{2+}$ EPR signals have been the subject of less study. This is because the detergent treatment used to isolate PSII in plants and the low pH used to stabilized Mn_4Ca cluster [44] appears to be detrimental to Q_B. It is possible that the low pH procedure could result in the loss of the native carbonate/bicarbonate ligand to the iron (the pKa of bicarbonate/carbonic acid is 6.4). Nevertheless, $Q_B^{\bullet-}Fe^{2+}$ signals have been reported in plant PSII on rare occasions in which Q_B integrity is conserved in standard preparations [10,39,45], and when efforts were made to conserve bicarbonate [46]. In the cyanobacteria however, $Q_B^{\bullet-}Fe^{2+}$ EPR signals are routinely detected, thus, Q_B seems more stable to both the detergent used and the pH [47,48]. The native $Q_B^{\bullet-}Fe^{2+}$ EPR signal has a very similar line shape to that observed for the native $Q_A^{\bullet-}Fe^{2+}$ [48].

Fufezan et al. noted the presence of an additional functional quinone in *T. elongatus* PSII core preparations [48]. An additional quinone was also reported in quinone quantification studies in similar preparations [49] and was detected in the most recent crystallographic model of PSII and designated Q_C [23]. Mechanistic evidence for an additional quinone binding site in PSII from plants had already been obtained from studies of Cytochrome b559 (Cyt b_{559}) [50,51].

In the present work we have used EPR to study the effect of formate binding on PSII using cyanobacterial preparations that have functional Q_B and Q_C prior to formate addition.

2. Materials and methods

2.1. Culture conditions

A strain of *T. elongatus* with a histidine tag on the CP47 protein of PSII was engineered as described in supplementary information. Cells of the transformed strain were grown in a rotary shaker (120 rpm) at 45 °C under continuous illumination using fluorescent white lamps of intensity of about 80 μmoles photons m^{-2} s^{-1}. Cells were grown in a DTN-medium [52] in a CO_2-enriched atmosphere. For maintenance, the cells were grown in the presence of kanamycin (40 μg ml^{-1}). For PSII preparations, the cells were grown in 3 L flasks (1 L culture).

2.2. PSII preparation

PSII core complexes were prepared as described in [53] using a protocol based on [54] with the following modifications. The concentrations of betaine in all buffers used here was 1 M instead of 1.2 M and the concentration of *n*-dodecyl-β-maltoside used in the elution buffer "buffer 3" was 0.06% (w/v) instead of 0.10% (w/v). The eluted fraction from the nickel column was concentrated and washed using Millipore Ultrafree-15 centrifugal filters. Oxygen evolution was measured under continuous light at 27 °C in a Clark-type oxygen electrode (Hansatech) with saturating white light. The oxygen evolution activity of the PSII core complexes was ~3500 μmol $O_2 \cdot mg^{-1} \cdot Chl/h$. Samples were stored in liquid nitrogen in the storage buffer (10% glycerol, 40 mM MES pH 6.5, 1 M betaine, 15 mM $MgCl_2$ and 15 mM $CaCl_2$).

2.3. Formate treatments

For EPR experiments the formate treatment was performed as follows. 120 μL aliquots of PSII (~1 mg Chl/ml) were dark-adapted for the time specified in the figure legends (either 1 or 12 h), then 160 mM final concentration of sodium formate in the storage buffer was added in the dark and the sample allowed to incubate for 30 min incubation at room temperature. Experiments in which the concentration and incubation time were varied demonstrated that these conditions were optimal for generating ~100% of the modified semiquinone–iron EPR signals (not shown). For oxygen evolution measurements 160 mM of sodium formate was added to PSII at 5 μg Chl/ml, and the sample was then incubated for 30 min at room temperature. The O_2 evolving activity decreased to 20% under these conditions and was restored to 60% by addition of 50 mM bicarbonate.

These formate-induced changes in activity are reported in the literature (e.g. [55]). The addition of 160 mM NaCl had no affect on oxygen evolution. In all the experiments shown here sodium formate was added as a 1 M stock in storage buffer.

2.4. Chemical reduction treatments

Chemical reduction of the 120 µL aliquots of PSII (~1 mg Chl/ml) with ascorbate was performed using two methods (see figure legends). (1) Sodium ascorbate in storage buffer (300 mM stock) was added to the sample in the EPR tube in darkness to give a final concentration of 10 mM. The sample was then incubated for 10 min at room temperature prior to freezing. (2) DAD in DMSO (30 mM stock solution) was added to the sample in the EPR tube in darkness to give a final concentration of 1 mM and then sodium ascorbate in storage buffer was added to give a final concentration of 10 mM. The sample was then incubated for 30 min at room temperature before freezing the sample (see below). Dithionite reduction was performed by addition of sodium dithionite to the sample in the EPR tube to give a final concentration of 30 mM using a 500 mM stock solution made up in degassed storage buffer.

2.5. EPR measurements

EPR spectra were recorded using a Bruker Elexsys 500 X-band spectrometer equipped with standard ER 4102 resonator and Oxford Instruments ESR 900 cryostat. Instrument settings were: microwave frequency 9.4 GHz, modulation frequency 100 kHz. All other settings were as indicated in the figure legends. 120 µl aliquots of PSII cores (~1 mg Chl/ml) in the same buffer used for storage were loaded into 4 mm outer diameter quartz EPR tubes. The samples were manipulated under dim-green light and then incubated in complete darkness for 1 h (short-dark adaptation) or 12 h (long-dark adaptation). The EPR samples were frozen in a dry-ice/ethanol bath at 200 K. Samples were degassed by pumping at 200 K and then filled with helium gas. EPR tubes were then transferred to liquid nitrogen prior to the EPR measurements being made. Samples were handled in darkness.

2.6. Illumination conditions

Flashes were performed using a frequency-doubled Nd:YAG laser (Spectra Physics, 7 ns fwhm, 550 mJ, 532 nm) at room temperature. After flashing, samples were rapidly frozen (1-2 s) in a dry-ice/ethanol bath at 200 K followed by storage in liquid nitrogen. The laser flash used was saturating under these conditions.

Low-temperature red-light illuminations were performed in an unsilvered dewar using either liquid nitrogen (77 K) or a dry-ice/ethanol bath at 200 K. 77 K illuminations were performed for 30 min in order to reduce $Q_A^{\bullet-}Fe^{2+}$ and oxidize Cyt b_{559} to near completion, as verified by EPR. Illuminations at 200 K for ~20 sec generated ~100% S_2 manganese multiline signal. Continuous illuminations were performed using an 800 W halogen lamp. The light was filtered through 3 cm of water, Calflex IR heat filters and a long-band pass filter (RG-670 nm).

For multiple photochemical turnover experiments, separate samples were used for 0, 1, 2 and 3 turnovers. The samples were treated with sodium ascorbate after a long dark adaptation (see above). A photochemical turnover was performed by illuminating a sample for 30 min at 77 K. Samples were then thawed and incubated for 10 min at room temperature, this allowed: (i) electron transfer to be completed on the electron acceptor side, i.e. $Q_A^{\bullet-}$ to Q_B, or $Q_A^{\bullet-}$ to $Q_B^{\bullet-}$, associated protonation reactions and the exchange of Q_BH_2 when possible; and (ii) the reduction of the oxidized Cyt b_{559} by ascorbate as verified by EPR. When a second or third turnover was required, further low temperature illumination/thawing cycles were given. Sodium formate (final concentration 160 mM) was added to samples which had undergone 0, 1, 2 and 3 turnovers and then incubated for 30 min at room temperature in darkness. Samples were then frozen and their EPR spectra recorded.

2.7. EPR simulations

Spectral simulations were performed as described in [34]. The Spin Hamiltonian (10 x 10 matrix) was solved numerically using: (i) Scilab-4.4.1, an open source vector-based linear algebra package (www.scilab.org); and (ii) the EasySpin package [56] in MATLAB. To broaden the comparison we also simulated $Q_A^{\bullet-}Fe^{2+}$ and $Q_B^{\bullet-}Fe^{2+}$ signals from wild type of *Rhodopseudomonas viridis* chromatophores. Biochemical preparation and EPR conditions for the *R. viridis* were as described in Ref. [57]

3. Results

3.1. The formate-modified $Q_B^{\bullet-}Fe^{2+}$ EPR signal

Fig. 1A shows the EPR spectrum measured at 4.5 K of untreated PSII core complexes isolated from *T. elongatus* after short dark-adaption. A weak broad signal was observed at $g=1.73$ that is characteristic of the $Q_B^{\bullet-}Fe^{2+}$ complex [48]. The $Q_B^{\bullet-}Fe^{2+}$ complex has a second turning point at $g=1.95$ that is not readily observed at this temperatures (see [34]) but which can be seen more easily at higher temperatures [48] (see Fig. 6). The addition of sodium formate alters the $Q_B^{\bullet-}Fe^{2+}$ signal (Fig. 1B). The native signal as described above is replaced by a new signal centered at g~1.84 that is similar to semiquinone–iron signals observed in purple bacteria reaction centers [58,59]. A similar signal has also been observed for the formate-modified $Q_A^{\bullet-}Fe^{2+}$ complex in plant and cyanobacterial PSII [38,40,41,60].

Under the experimental conditions used here, no $Q_A^{\bullet-}$ is expected to be reduced prior to the addition of formate. In contrast, $Q_B^{\bullet-}$ is expected to be present in a significant fraction of centers (~40%) after a short-period of dark-adaptation in *T. elongatus* [48]. Thus it is probable that this new signal (Fig. 1B) arises from the formate-modified $Q_B^{\bullet-}Fe^{2+}$, where formate has displaced the exogenous bicarbonate/carbonate ligand of the Fe^{2+}. The new semiquinone–

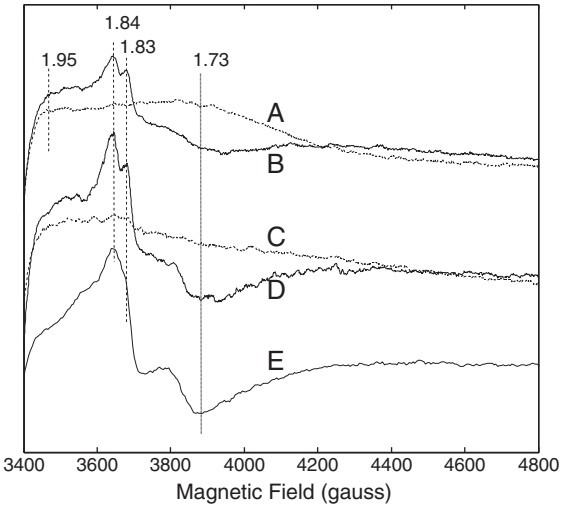

Fig. 1. EPR signals present in formate-treated PSII from *T. elongatus*. (A) Short-dark adapted (1 h) PSII. (B) After formate addition to the sample shown in A. (C) Formate added to a long-dark adapted PSII. (D) One saturating laser flash at room temperature given to the long dark-adapted sample shown in C. (E) Spectrum attributed to formate-modified $Q_A^{\bullet-}Fe^{2+}$ generated by 30 min illumination at 77 K in a long-dark adapted PSII sample. Some g-values of features mentioned in the text are shown. Instrument settings: microwave power: 20 mW, modulation amplitude: 25 gauss, temperature: 4.5 K.

iron signal described above was absent when formate was added to a sample that had been dark-adapted for 12 h (Fig. 1C). Incubation for 12 h in the dark at room temperature is known to result in the almost complete loss of $Q_B^{\bullet-}$ Fe^{2+} [48]. This result is consistent with the assignment of the signal in Fig. 1B to a formate-modified form of $Q_B^{\bullet-}Fe^{2+}$.

Fig. 1D shows the EPR signal obtained after a single saturating flash was given to a long dark-adapted sample (Fig. 1C) at room temperature. The photo-induced signal is similar to that seen in Fig. 1B. Excitation of dark-adapted PSII by a single saturating flash is expected to generate the $S_2Q_B^{\bullet-}$ state. This result further supports the assignment of this new signal to the formate-modified $Q_B^{\bullet-}Fe^{2+}$ complex. The size of the $Q_B^{\bullet-}Fe^{2+}$ signal in Fig. 1D is approximately double that of the signal seen for the short dark-adapted sample (Fig. 1B). This suggests that formate does not affect the yield of $Q_B^{\bullet-}$ formation on the first flash and is consistent with earlier studies of bicarbonate depletion/formate addition (e.g. [28–33]). In this experiment the contribution from the overlapping S = ½ multiline signal from S_2 is minimized by the choice of EPR conditions used for the measurement (low temperature and high microwave power). When S_2 is formed in centers containing TyrD, the S_2 state is reduced back to the S_1 state and $TyrD^{\bullet}$ is formed [61]. This occurs in the seconds timescale through the equilibrium between the intervening electron carriers (P_{680}, TyrZ) (reviewed in [62]). This also contributes to the low intensity of the S_2 signal in Fig. 1D.

Control measurements (see Fig. S2 in supporting information) showed that the addition of formate did not significantly alter the electron donor side function on the first photochemical turnover. The S_2 multiline signal [63] generated by 200 K illumination [64] had almost the same amplitude in control and formate-treated samples, ±20% (Fig. S2 in supporting information). This is in marked contrast to the situation in plant PSII where it was concluded that acceptor side effects of formate were matched by donor side inhibition [65,66] but see however [67]. The discrepancy is most likely due to species differences and/or biochemical conditions.

Fluorescence yield experiments were performed on samples before and after the addition of formate to rule out the possibility that formate addition led to $Q_A^{\bullet-}$ reduction in the short dark-adapted samples, perhaps by a change in the $Q_AQ_B^{\bullet-} \leftrightarrow Q_A^{\bullet-}Q_B$ equilibrium. The addition of formate increased the F_0 level by less than 1% of the F_{max} (see Table 1 in supporting information). In addition, thermoluminescence experiments in the presence of formate indicated that $S_2Q_B^{\bullet-}$ recombination occurs on the first flash; no evidence for $S_2Q_A^{\bullet-}$ recombination was seen (not shown). These results show that formate addition does not generate formation of a significant fraction of $Q_A^{\bullet-}$ from $Q_B^{\bullet-}$ and further support the assignment of the new EPR signal (Fig. 1B) to formate-modified $Q_B^{\bullet-}Fe^{2+}$.

Fig. 1E shows the EPR signal generated by illumination of a long dark-adapted PSII sample at 77 K for 30 min. Illumination at this temperature is known to generate $Q_A^{\bullet-}$ in most centers [68]. The observed $Q_A^{\bullet-}Fe^{2+}$ signal (Fig. 1E) has the same *g*-values (a peak at $g = 1.84$ and a trough at $g \sim 1.73$) and line-shape as seen in PSII from higher plants [38] and as reported earlier in *T. elongatus* [40,41]. The signal generated after one flash (Fig. 1D), which is attributed to $Q_B^{\bullet-}Fe^{2+}$, is similar to that of $Q_A^{\bullet-}Fe^{2+}$ (Fig. 1E) but it has an additional resolved secondary peak at $g \sim 1.83$. These small changes in the line-shape of the two signals are reminiscent of those that distinguish the $Q_A^{\bullet-}Fe^{2+}$ and $Q_B^{\bullet-}Fe^{2+}$ signals in purple bacteria [59,69,70].

3.2. Formate-treated PSII illuminated by a series of flashes

The left panel of Fig. 2 shows the effect of a series of flashes on long dark-adapted PSII that was subsequently treated with formate. Fig. 2A, the zero flash sample showed no signal. After one flash (Fig. 2B) the $Q_B^{\bullet-}Fe^{2+}$ was formed in the majority of the centers (~80%, this is obtained from an estimate of the miss factor derived from the size of the signal present after the second flash). Fig. 2C shows the sample that was excited by two flashes. In this case, the EPR signal was significantly smaller than that seen after 1 flash (Fig. 2B). The residual $Q_B^{\bullet-}Fe^{2+}$ observed maybe attributed to: (i) the centers that did not turnover on the first flash because of photochemical misses but which did turnover on the second flash; and (ii) those centers that did turnover on the first flash but not on the second flash, again because of misses. The marked decrease in amplitude on the second flash is similar to that expected for untreated PSII. This indicates that the yield of electron transfer from $Q_A^{\bullet-}$ to Q_B and from $Q_A^{\bullet-}$ to $Q_B^{\bullet-}$ is not greatly affected by formate treatment. In contrast on the third and subsequent flashes the EPR spectra indicate the gradual accumulation of an EPR signal with peaks at $g = 1.84$ with additional features at $g = 1.81$ and $g = 1.68$ (Fig. 2D and E).

In the right panel of Fig. 2 each of the samples that had been flashed at room temperature (Fig. 2 left panel), were then illuminated at 77 K. Under these conditions the final electron donors are the chlorophyll(s), the carotenoid(s) or Cyt b_{559}, known collectively as the side-pathway donors [71]. Fig. 2F shows the one flash sample (Fig. 2B) after illumination at 77 K. The EPR signal intensity of the

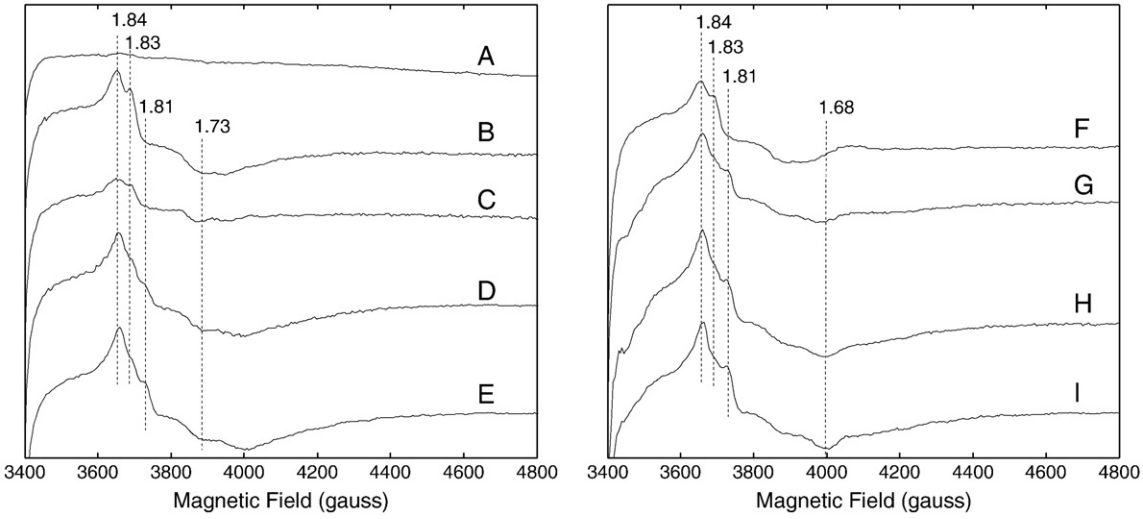

Fig. 2. The effect of a flash series on the formate-treated PSII. PSII samples were dark-adapted for 12 h. A series of 0, 1, 2, 3, 4 flashes were then given. The corresponding spectra are shown in the left panel and labeled as A, B, C, D and E respectively. In the right panel, the spectra labeled F, G, H and I correspond to the samples used to obtain spectra B, C, D and E, respectively, but after a 77 K illumination. Instrument settings were the same as in Fig. 1.

semiquinone–iron signal decreased upon 77 K illumination. This effect is more marked under comparable conditions in Fig. 3 (see below). This is attributed to the formation of a $Q_A^{\bullet-}Fe^{2+}Q_B^{\bullet-}$ biradical species that does not show an EPR signal in this region. A similar situation occurs in purple bacterial centers when the same state is formed [69,72]. The theoretical rationale for this will be discussed elsewhere (Cox et al., in preparation).

In Fig. 2F the remaining signal is a mixture of $Q_A^{\bullet-}Fe^{2+}$ and $Q_B^{\bullet-}Fe^{2+}$ present in separate centers. Illumination of samples that had been pre-flashed by 2, 3 or 4 flashes prior to low temperature illumination (Fig. 2G, H and I) showed an increase in the EPR intensities and the signal formed is broad and has features at $g=1.84$, $g=1.81$ and $g=1.68$. This is the same signal which appeared after 3 and 4 flashes prior to low temperature illumination (Fig. 2D and E). Given that this signal is formed at low temperature, it seems likely that it arises from $Q_A^{\bullet-}$ even though it is unlike the well-known formate-modified $Q_A^{\bullet-}Fe^{2+}$ signal (Fig. 1E) [38]. In Fig. 2 this new signal is seen when three or more turnovers have occurred: i.e. after 3 or more flashes at room temperature or after 2 or more flashes at room temperature plus an illumination at 77 K.

3.3. EPR signals formed after a series of photochemical turnovers at low temperature

In Fig. 2 it was shown that in formate-treated PSII the typical period-of-two flash dependence in the $Q_B^{\bullet-}$ concentration could be observed for the first two flashes but its reappearance on the third flash was inhibited. To demonstrate more extensive period of two amplitude oscillations in the $Q_B^{\bullet-}Fe^{2+}$ signal we performed experiments in which the $Q_A^{\bullet-}$ to $Q_B/Q_B^{\bullet-}$ electron transfer steps were allowed to occur *before* adding the formate. Fig. 3 (left panel) shows variations in the size of the $Q_B^{\bullet-}Fe^{2+}$ EPR signal depending on the number of photochemical turnovers when formate was added *after* the turnovers had occurred. Because of the long incubation time needed for formate to bind and the occurrence of charge recombination during this time, this experiment could not be done by addition of formate after a series of flashes. Instead photochemical turnovers were generated using a protocol involving low temperature illumination (77 K) of ascorbate-reduced PSII followed by thawing (for details, see material and methods). The increase in the size of the signal on turnovers 1 and 3 (Fig. 3B and D) is characteristic of Q_B function and further supports the assignment of the signal to the formate-modified $Q_B^{\bullet-}Fe^{2+}$ state.

The right panel of Fig. 3 shows EPR spectra obtained from the same samples used for the experiments used for the multiple turnover experiments (Fig. 3 left panel) but recorded directly after an additional illumination at 77 K. Fig. 3E shows the formation of a formate-modified $Q_A^{\bullet-}Fe^{2+}$ signal in a dark-adapted sample. Fig. 3F shows the effect of illumination at 77 K of a sample that already contained the formate-modified $Q_B^{\bullet-}Fe^{2+}$ state in a significant fraction of centers. The resulting signal has a smaller amplitude (i.e. $Q_B^{\bullet-}Fe^{2+}$ signal is lost) (Fig. 3F) and is more reminiscent of a residual formate-modified $Q_A^{\bullet-}Fe^{2+}$ signal. These effects can be explained in the same way as those in Fig. 2F: the $Q_A^{\bullet-}Fe^{2+}Q_B^{\bullet-}$ biradical state was formed in those centers in which $Q_B^{\bullet-}Fe^{2+}$ was present prior to the 77 K illumination and this state exhibits no (or a small) EPR signal in this region. The remaining signal seen upon illumination represents formation of $Q_A^{\bullet-}Fe^{2+}$ in those centers lacking $Q_B^{\bullet-}$ prior to 77 K illumination. By comparison to the $Q_A^{\bullet-}Fe^{2+}$ signal in Fig. 3E, this fraction is estimated to represent ~25% of centers.

Fig. 3G shows the result of a 77 K illumination given to a sample that had undergone two turnovers and should have passed two electrons already to Q_B in the majority of centers. Because of inefficiencies in the turnover protocol some centers do show formate-modified $Q_B^{\bullet-}Fe^{2+}$ prior to the 77 K illumination, however this is in a small minority of centers. As seen earlier (Fig. 2), instead of the standard formate-modified $Q_A^{\bullet-}Fe^{2+}$ EPR signal (e.g. Fig. 3E), a new broader signal (with peaks at $g=1.84$, and $g=1.81$ and a trough at $g=1.68$) is observed (see Fig. 2). A similar signal was seen after 77 K illumination of a sample that had undergone three turnovers (Fig. 3H). The data in Fig. 3 confirm the association of the new signal with a formate-modified $Q_A^{\bullet-}Fe^{2+}$ state in centers in which two (or more) electrons have already arrived at the secondary acceptor.

3.4. The new formate modified $Q_A^{\bullet-}Fe^{2+}$ signal: effects of light, reductants and inhibitors

The new broad signal was also seen when a formate-treated sample was frozen under illumination (Fig. 4B) or frozen in the dark immediately after illumination (not shown). This treatment should fully reduce Q_B, Q_C (when present and if reducible) and trap $Q_A^{\bullet-}$ in the reduced form. Fig. 4B shows that the new signal formed does not resemble the usual $Q_A^{\bullet-}Fe^{2+}$ signal (trace 4A). It has a significantly

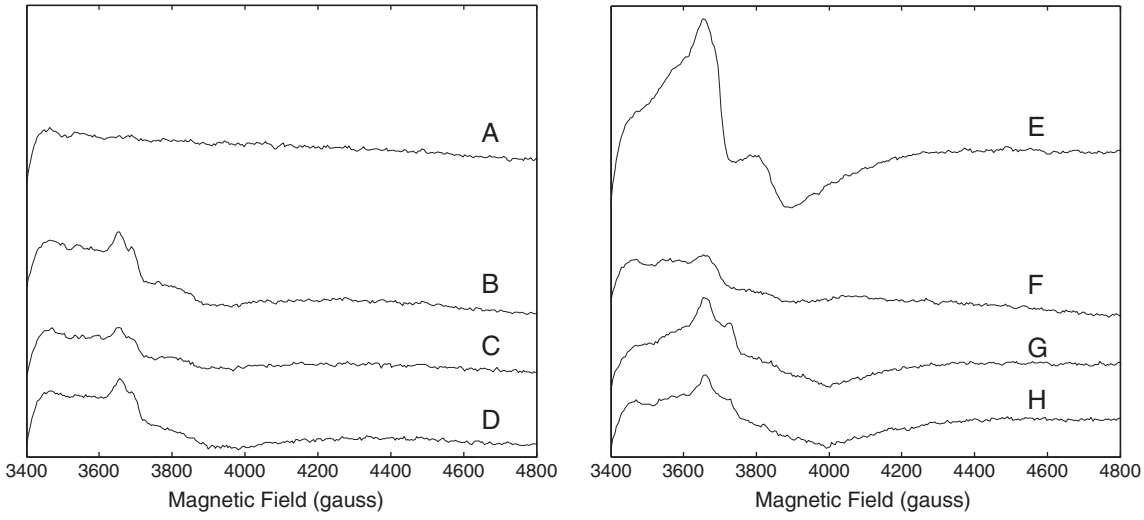

Fig. 3. The formate-modified signal monitored with different $Q_B^{\bullet-}$ concentrations induced by 0, 1, 2 or 3 photochemical turnovers occurring *prior* to formate addition. See the text and material and methods for more experimental details. In the left panel, A, B, C and D represent the formate-induced EPR signal after 0, 1, 2 and 3 photochemical turnovers respectively. In the right panel, E, F, G and H show the samples shown in the left panel, A, B, C and D, respectively, but after a 77 K illumination. Instrument settings were the same as in Fig. 1.

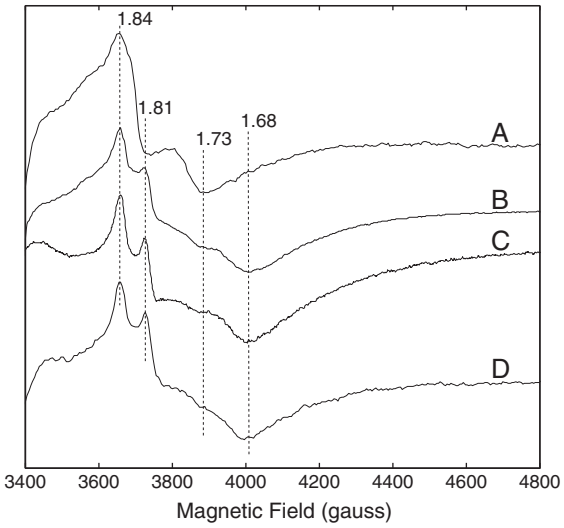

Fig. 4. The formate-modified $Q_A^{\bullet-}Fe^{2+}$ EPR signals generated in formate-treated PSII under a range of conditions: (A) illumination at 77 K of the 12 h dark-adapted PSII showing the usual $Q_A^{\bullet-}Fe^{2+}$ formate-induced signal as reference; (B) freezing under illumination; (C) dithionite reduction in the dark; (D) 77 K illumination of a sample reduced by DAD/ascorbate. Instrument settings were the same as in Fig. 1.

different line-shape with a peak at $g=1.81$ and a trough at $g=1.68$. The same signal is formed in formate-treated samples when reduced with dithionite in the dark (Fig. 4C) and also when pre-reduced by DAD and sodium ascorbate and then illuminated at 77 K (Fig. 4D). Dithionite is expected to fully reduce Q_B to Q_BH_2 and singly reduce Q_A in the dark. Similarly, DAD/ascorbate treatment is able to doubly reduce Q_B to Q_BH_2 in fraction of centers, and subsequent illumination at 77 K is expected to result in formation of $Q_A^{\bullet-}$. Hence, both of these chemically modified samples represent the $Q_A^{\bullet-}Fe^{2+}Q_BH_2$ state (or possibly one of its deprotonated forms $Q_A^{\bullet-}Fe^{2+}Q_BH^{\bullet-}$ or $Q_A^{\bullet-}Fe^{2+}Q_B^{2\bullet-}$).

Fig. 5B and C show the signals generated in formate-treated PSII in the presence of DCMU after freezing under illumination or reduced by dithionite, respectively. Both conditions should give rise to $Q_A^{\bullet-}Fe^{2+}$. These signals are virtually indistinguishable from each other and similar to that formed by low temperature illumination in the absence

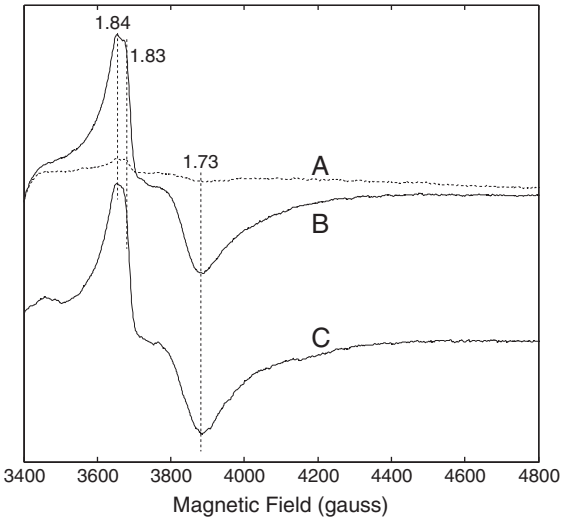

Fig. 5. Effect of DCMU on formate-treated, long dark-adapted PSII. (A) The signal present in the dark. (B) The signal formed after freezing under illumination. (C) The signal formed by reduction with dithionite. DCMU was prepared in DMSO (the concentration of the stock solution was 1 mM) was added to the sample in the EPR tube in darkness to give a final concentration of 50 μM. Instrument settings were the same as in Fig. 1.

of DCMU (Fig. 1E). These results indicate that occupation of the Q_B site by the inhibitor DCMU prevents the formation of the new broad signal.

When the PSII was treated with dithionite in the presence of ANT2p the modified $Q_A^{\bullet-}Fe^{2+}$ broad signal was converted to the unmodified $Q_A^{\bullet-}Fe^{2+}$ signal (Fig. S3). Similarly when the redox mediator indigodisulfonate ($E_m=-125$ mV), or the anion, azide, were added to dithionite reduced PSII, the modified signal showed partial reversion to the usual $Q_A^{\bullet-}Fe^{2+}$ signal (Fig. S3).

Fig. 6 shows an experiment in which DAD and sodium ascorbate were used as a reducing treatment. In the control sample without formate, the $Q_B^{\bullet-}$ was present in the majority of centers as indicated by the large $Q_A^{\bullet-}Fe^{2+}Q_B^{\bullet-}$ signal generated at $g=1.66$ upon illumination at 77 K [47,48]. This spectrum of the native $Q_A^{\bullet-}Fe^{2+}Q_B^{\bullet-}$ state (Fig. 6B) shows almost no overlap from the typical $Q_A^{\bullet-}Fe^{2+}$ signal at $g=1.95$, indicating that $Q_B^{\bullet-}$ was present in nearly all the centers prior to illumination at 77 K.

In the right panel the formate-modified $Q_B^{\bullet-}Fe^{2+}$ signal was formed in the presence of DAD/ascorbate (Fig. 6C). While the size of the signal seems to vary from experiment to experiment, illumination at 77 K resulted in formation of the new broad $Q_A^{\bullet-}Fe^{2+}$ signal. This was the case even when the formate-modified $Q_B^{\bullet-}Fe^{2+}$ signal was small. Given the assignment of the new signal to $Q_A^{\bullet-}Fe^{2+}$ in the presence of a two-electron reduced form of Q_B, this observation indicates that DAD/ascorbate is capable of doubly reducing Q_B in at least a fraction of the formate-treated PSII, while the untreated PSII was reduced only to the $Q_B^{\bullet-}$ level. This may indicate that the potentials of the redox couples associated with Q_B are shifted in the presence of formate, resulting in a less thermodynamically stable $Q_B^{\bullet-}$ state. Redox titrations are planned to test this.

We note that in the spectrum of native $Q_B^{\bullet-}Fe^{2+}$ in Fig. 6B there is a strong sharp feature at $g\sim2.00$, in addition to the typical features at $g=1.95$ and a broad signal at $g=1.71$ [48]. This new feature arises from $Q_B^{\bullet-}Fe^{2+}$ and is detected here because the TyrD$^{\bullet}$ signal is absent due to reduction by the DAD/ascorbate. This, and a corresponding signal in $Q_A^{\bullet-}Fe^{2+}$ will be the subject of a future publication. The $g=2.00$ signal from $Q_B^{\bullet-}Fe^{2+}$ can also be seen in the TyrD-less mutant (Boussac et al. personal communication).

3.5. Simulations of the semiquinone–iron EPR signals

Spectral simulations of the semiquinone–iron signal seen in formate treated PSII were performed using the Spin Hamiltonian formalism. The semiquinone–iron signal seen in purple bacteria is well understood from a theoretical standpoint [59]. The strong turning point at $g\sim1.8$ can be considered the intersection of two signals that arise from the two lowest Kramer's doublets of the quinone–iron spin manifold (for full discussion see [59]). The interaction of the non-heme iron ($S=2$) and semi-quinone, $Q_A^{\bullet-}$ ($S=½$) was described as follows. A basis set that describes the Fe-semiquinone ($Q^{\bullet}$, $S_Q=½$) spin manifold can be built from the product of the eigenstates of the two interacting spins. These are expressed in terms of three quantum numbers, $|S,\ m,\ s\rangle$. Where S is the total spin of the ground iron manifold ($S=2$), m is the iron magnetic sub-level ($m=-S, -S+1,\ldots, S-1, S$) and s is the semi-quinone sublevel ($s=-½,½$). Thus 10 basis vectors are required to span the spin manifold.

The Spin Hamiltonian appropriate for the $Q_A^{\bullet-}Fe^{2+}$ system, includes zero field (D, E), Zeeman (g_{Fe}, g_Q) and anisotropic exchange (J):

$$\mathcal{H} = D\left[\left(S_{FeZ}^2 - 1/3S_{Fe}(S_{Fe}+1)\right) + (E/D)\left(S_{FeX}^2 - S_{FeY}^2\right)\right] + \beta H\cdot g_{Fe}\cdot S_{Fe} + g_Q\beta H\cdot S - S_{Fe}\cdot J\cdot S_Q \quad (1)$$

Subsequent calculations assume the zero-field, Zeeman–iron and exchange tensors to be co-linear and g_Q to be scalar as in [59].

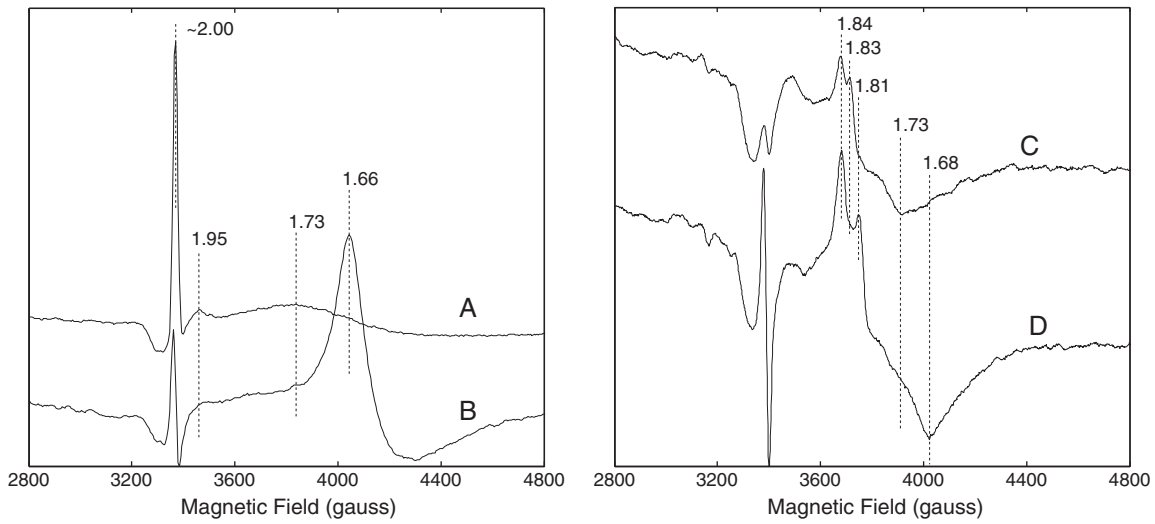

Fig. 6. Effect of DAD/ascorbate reduction on PSII in the presence and absence of formate. Left panel shows untreated PSII, (A) in the dark and (B) after illumination at 77 K. Right panel shows formate-treated PSII, (C) in the dark and (D) after illumination at 77 K. Instrument settings were the same as in Fig. 1, except for the temperature (5 K).

Estimates for all the Spin Hamiltonian parameters (D, E, g_{Fe}, g_Q and J) have been made in the species *R. sphaeroides*. The zero-field splitting of the non-heme iron, measured using static magnetisation, yielded values of D ~ 5 cm^{-1} (7.6 K^{-1}) and E/D ~ 0.25. The interaction between the quinone and the iron is axial and of the order of ~0.5 cm^{-1}. The structural homology between the PSII and purple bacteria and the strong similarity of the semiquinone iron signals observed suggest that the same theoretical approach is valid. The starting point for all optimized simulations reported here is the parameter set as determined for *R. sphaeroides*.

Table 1 shows the fitted parameters for simulations presented in Fig. 7. As a calibration, the variation amongst different purple bacteria was examined. *R. viridis* has virtually the same quinone–iron acceptor side complex as *R. sphaeroides* with the exception that *R. viridis* contains a menaquinone as Q_A instead of a ubiquinone. Only small differences for the simulated parameters were seen between the two species (Table 1). Both simulations (in *R. viridis* and *R. sphaeroides*) were of samples where *o*-phenanthroline was bound, displacing Q_B from its site. The addition of *o*-phenanthroline and other herbicides slightly narrows the signal of $Q_A^{\bullet-}Fe^{2+}$ and this has a minor affect on the parameters of the fitted lineshape (see [59]).

Simulation of the semiquinone–iron signals ($Q_A^{\bullet-}Fe^{2+}$ or $Q_B^{\bullet-}Fe^{2+}$) seen in formate-treated PSII are also very similar to those seen in purple bacteria with little variation in the coupling between the quinone and the iron and in zero-field splitting of the iron. However, the coupling interaction is rhombic rather than axial. This suggests that there is a small difference in for example the tensor geometries in PSII compared to purple bacteria. An analogous change in the tensor orientations of the system was observed in DFT calculations of iron–quinone model complexes based on crystallographic data from the bacterial reaction center and PSII [34]. No significant change was observed in the magnitude of the zero-field splitting of the iron, but small changes were seen for the orientation of the tensor coupling relative to the zero-field tensor (as estimated by the Fe hyperfine tensor). The $Q_B^{\bullet-}Fe^{2+}$ signal seen in *R. viridis* can also be modeled using the same parameters as used for formate-treated PSII ($Q_A^{\bullet-}Fe^{2+}$ or $Q_B^{\bullet-}Fe^{2+}$). The slightly different parameters used for $Q_B^{\bullet-}Fe^{2+}$ compared to $Q_A^{\bullet-}Fe^{2+}$ may reflect the slight asymmetry in the $Q_AFe^{2+}Q_B$ motif in *R. viridis*, as seen in its crystal structure [11].

A more significant change is observed for the new broad signal attributed to $Q_A^{\bullet-}Fe^{2+}Q_BH_2$. The spectrum of the $Q_A^{\bullet-}Fe^{2+}Q_BH_2$ state shown in Fig. 7 was corrected by subtraction of the unperturbed $Q_A^{\bullet-}Fe^{2+}$ signal (see figure caption). The corrected lineshape is reminiscent of the semiquinone iron signal ($Q_A^{\bullet-}Fe^{2+}$) of purple bacteria rather than those in PSII, with the peak-to-trough splitting the same as observed for *R. viridis* (~310 G). However, the turning point of $Q_A^{\bullet-}Fe^{2+}Q_BH_2$ is shifted to higher field by ~100 G compared to all the other semiquinone signals simulated. The fitted parameters show that this new signal is basically similar to that of "typical" g ~ 1.8 semiquinone–iron signals. The exchange interaction between the quinone and the iron is axial, with the x component being the smallest. It appears though that the zero-field splitting of the iron is significantly bigger (~2 K^{-1}). This solution is unlikely to be unique since the changes in the coupling between semiquinone and iron (in particular the J_Y component) and the changes in the zero-field splitting influenced the simulated spectrum in the same way. The fitted parameters presented represent the minimum changes to the *R. sphaeroides* solution that are required to reproduce the new spectrum.

In conclusion these simulations demonstrate that a significant change in the fitted parameters is required to simulate the $Q_A^{\bullet-}Fe^{2+}Q_BH_2$

Table 1
Optimized parameter set for the simulation of the semiquinone–iron complex signals.

	R. sphaeroides ($Q_A^{\bullet-}Fe^{2+}$)[b,c]	*R. viridis* ($Q_A^{\bullet-}Fe^{2+}$)[b]	PSII + formate ($Q_A^{\bullet-}Fe^{2+}$,$Q_B^{\bullet-}Fe^{2+}$) *R. viridis* ($Q_B^{\bullet-}Fe^{2+}$)[a]	PSII + formate ($Q_A^{\bullet-}Fe^{2+}Q_BH_2$)
J_{1X} (K^{-1})	−0.13	−0.154	−0.103	−0.193
J_{1Y} (K^{-1})	−0.58	−0.689	−0.733	−1.003
J_{1Z} (K^{-1})	−0.58	−0.630	−0.496	−1.008
$J_{1(ISO)}$ (K^{-1})	−0.43	−0.491	−0.444	−0.73
D (K^{-1})	7.6	7.560	7.740	9.82
E/D	0.25	0.253	0.250	0.270

[a] *R. sphaeroides* ($Q_A^{\bullet-}Fe^{2+}$) taken from Butler et al. [59].
[b] In the presence of *o*-phenanthroline.
[c] g_{Fe} tensor values fixed to those reported in [59].

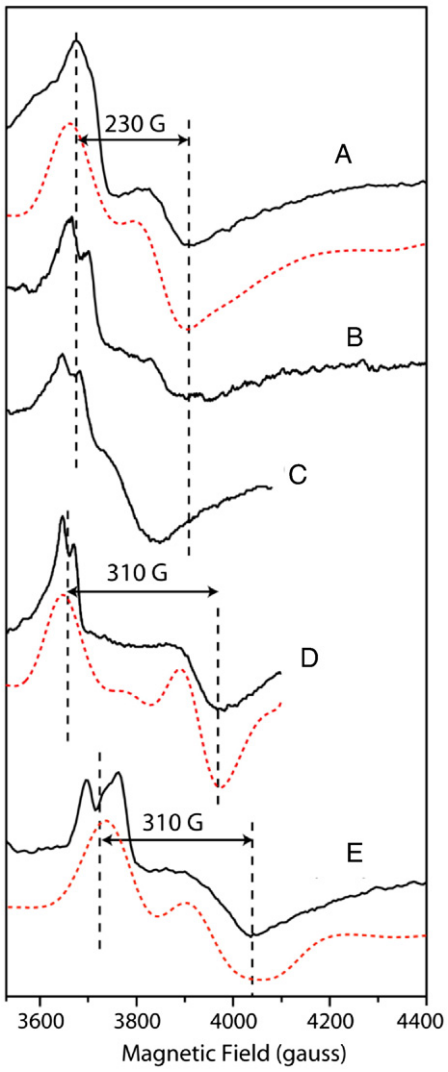

Fig. 7. Simulation of the semiquinone–iron complex signals seen in purple bacteria and PSII. (A) the $Q_A^{\bullet-}Fe^{2+}$ signal seen in PSII; (B) the $Q_B^{\bullet-}Fe^{2+}$ signal seen of PSII; (C) the $Q_B^{\bullet-}Fe^{2+}$ signal in *R. viridis*; (D) the $Q_A^{\bullet-}Fe^{2+}$ signal observed in *R. viridis* were *o*-phenanthroline was added (see [57]); (E) the modified $Q_A^{\bullet-}Fe^{2+}Q_BH_2$ state seen in PSII. This spectrum has been corrected by subtraction of the unperturbed $Q_A^{\bullet-}Fe^{2+}$ signal. It is estimated that the unperturbed $Q_A^{\bullet-}Fe^{2+}$ state accounts for ~20–30% of centers under the conditions where a maximal modified $Q_A^{\bullet-}Fe^{2+}Q_BH_2$ signal was observed. The offset dashed lines show spectral simulations of the EPR lineshape using the Spin Hamiltonian formalism discussed in the text.

quinone–iron complex and this change is much larger than the variation seen in all of the g~1.8 semiquinone–iron signals seen in a range of species in the presence and absence of herbicides.

4. Discussion

4.1. An EPR signal from $Q_B^{\bullet-}Fe^{2+}$ in the presence of formate

Here we report an EPR signal that we attribute to formate-modified $Q_B^{\bullet-}Fe^{2+}$ state. This assignment is based on a series of observations and arguments. (i) The signal is similar but not identical to the signal observed for the $Q_A^{\bullet-}Fe^{2+}$ in the presence of formate [38]. (ii) The differences between the new signal and the formate modified $Q_A^{\bullet-}Fe^{2+}$ signal in PSII are similar to those that differentiate the $Q_A^{\bullet-}Fe^{2+}$ and $Q_B^{\bullet-}Fe^{2+}$ signals in purple bacterial reaction centers [59,69,70]. (iii) The EPR signal is formed upon addition of formate to a short dark-adapted sample (Fig. 1) and $Q_B^{\bullet-}$ is known to be stable in the native system (i.e. bicarbonate/carbonate bound) after short dark-adaption [48]. (iv) The formation of the EPR signal does not result in an increase in fluorescence yield (Table 1 in supplementary information) and thus the signal cannot be attributed to a modified form of $Q_A^{\bullet-}$. (v) The new signal is relatively stable but decays after 12 h of dark adaptation (Fig. 1) as expected from $Q_B^{\bullet-}$ [48]. Since we observed that $TyrD^{\bullet}$ decays in a significant fraction of centers during the long dark adaptation (not shown), and since evidence exists for $TyrD^{\bullet}$ $Q_A^{\bullet-}$ recombination at room temperature [73], the slow $Q_B^{\bullet-}$ decay may at least in part reflect $TyrD^{\bullet}$ $Q_B^{\bullet-}$ recombination. (vi) When the signal was absent, a single flash reformed the new signal with double the amplitude of that present in a short (1 h) dark-adapted sample (Fig. 1). (vii) The signal is much smaller on the second flash, as expected of $Q_B^{\bullet-}$ (Fig. 2). Taking into account the usual photochemical miss factor, we estimate that $Q_B^{\bullet-}$ is present in ~80% of centers after 1 flash. Thus the signal present in the short dark-adapted sample is estimated to be approximately 40%. These estimates are similar to those for $Q_B^{\bullet-}Fe^{2+}$ in untreated PSII in comparable conditions [48]. On the third flash however the $Q_B^{\bullet-}Fe^{2+}$ signal did not increase in intensity. Instead a new signal attributed to $Q_A^{\bullet-}Fe^{2+}$ in the presence of a two electron reduced form of Q_B was seen. (viii) The formate-modified $Q_B^{\bullet-}Fe^{2+}$ signal shows a period-of-two oscillation in its amplitude when formate is added *after* photochemical turnovers have occurred (Fig. 3). (ix) The signal can be formed by reduction of a formate-treated sample with DAD/ascorbate, conditions which generate a high concentration of $Q_B^{\bullet-}$ in the native system (Fig. 6).

These lines of evidence present a convincing case for the assignment of this EPR signal to assignment to a formate-modified $Q_B^{\bullet-}Fe^{2+}$ state. This new signal is easy to detect and should be useful for measuring the presence of $Q_B^{\bullet-}$. The maximum signal intensity seen in these studies is less (by around a factor of 2 based on the flash experiments) than that seen for the $Q_A^{\bullet-}Fe^{2+}$ signal in the same samples. This may be partially explained by inefficiencies in electron transfer, (e.g. less than 100% occupancy by Q_B, miss factors…etc.), however it also represents an intrinsically smaller signal from this state. A similar situation was seen for $Q_B^{\bullet-}Fe^{2+}$ in *R. viridis*, where the $Q_B^{\bullet-}Fe^{2+}$ signal also shows a greater splitting of the main peak [70] as shown here for PSII.

4.2. The $Q_A^{\bullet-}Fe^{2+}Q_B^{\bullet-}$ state in formate-treated PSII

In untreated PSII the $Q_A^{\bullet-}Fe^{2+}Q_B^{\bullet-}$ state gives rise to a strong signal at $g=1.66$ (Fig. 6B) [46–48]. Here we show that when formate is bound, the $Q_A^{\bullet-}Fe^{2+}Q_B^{\bullet-}$ state does not give rise to a signal at $g=1.66$. Instead the signal intensity at $g=1.84$ decreases while the shape of the residual signal is attributable to residual $Q_A^{\bullet-}Fe^{2+}$, and perhaps $Q_B^{\bullet-}Fe^{2+}$ present in a very small fraction of centers where $Q_A^{\bullet-}$ is not formed by 77 K illumination [68]. The absence of an EPR signal in this region in the $Q_A^{\bullet-}Fe^{2+}Q_B^{\bullet-}$ state in formate-treated PSII is a further similarity with the purple bacterial reaction centers (see [69,72]). The absence of a signal in this region from the $Q_A^{\bullet-}Fe^{2+}Q_B^{\bullet-}$ state can be understood based on simulations of the spectra and theoretical considerations (Cox et al, in preparation).

4.3. A new formate-modified $Q_A^{\bullet-}Fe^{2+}$ EPR signal: $Q_A^{\bullet-}Fe^{2+}Q_BH_2$?

The second novel EPR signal described here seems to represent $Q_A^{\bullet-}Fe^{2+}$ modified not only by formate but also by the presence of a two-electron reduced form of Q_B. This signal is broader than the usual formate-modified $Q_A^{\bullet-}Fe^{2+}$ signal, with peaks at g~1.84 and g~1.81 and a marked trough at g~1.68. This new state can be generated in several ways in formate-treated PSII: (i) after 3 or more flashes at room temperature (Fig. 2D and E); (ii) by photo-generating $Q_A^{\bullet-}Fe^{2+}$ at low temperature after Q_B has been reduced by two electrons photochemically (Figs. 2 and 3 right panels) or chemically (Fig. 4); (iii) freezing under illumination (Fig. 4B) or immediately after illumination; and (iv) dithionite reduction (Fig. 4C). Furthermore, in the presence of the inhibitor DCMU it

was not possible to form the broad signal. These results indicate that the EPR signal from $Q_A^{\bullet-}Fe^{2+}$ is sensitive to the occupation of the Q_B site. It is already known that inhibitor binding in the Q_B site has a marked influence on the $Q_A^{\bullet-}Fe^{2+}$ EPR signal in PSII [74] and in the purple bacterial reaction centers [57,59]. However in the present work the $Q_A^{\bullet-}$ site is specifically and significantly modified by the presence of a two-electron reduced form of Q_B in its site. In contrast, in the purple bacterial reaction center, Butler et al. [59] reported that Q_BH_2 had only a small influence on the $Q_A^{\bullet-}Fe^{2+}$ signal.

This modified form of the formate-modified $Q_A^{\bullet-}Fe^{2+}$ signal in dithionite was not seen in earlier reports [38,40,41]. We suggest that this could reflect low occupancy of Q_B in these preparations. Early preparations of *T. elongatus* as used by van Mieghem, [40] lacked Q_B [21]. The small $Q_A^{\bullet-}Fe^{2+}Q_B^{\bullet-}$ EPR signal observed in the PSII preparation of *T. elongatus* [41] compared with our current material (see Fig. 6 and [48]), indicates that the PSII used in [41] had a low $Q_B^{\bullet-}$ concentration. The plant thylakoids used in Ref. [38] would be expected to have had native Q_B levels. However, much lower concentration of formate were used in [38]. An investigation of the concentration dependence of formate on the formation of the new $Q_A^{\bullet-}Fe^{2+}$ state may help understand these effects.

The presence of ANT2p, indigodisulfonate and azide, all resulted in a decrease of the new signal and a relative increase of the standard formate $Q_A^{\bullet-}Fe^{2+}$ signal (Fig. S3). It is not obvious why these diverse chemicals all had a similar effect. Redox, protonation, charge and binding effects can be imagined but further experimentation is required before this can be determined.

Based on the literature [33,75], the most likely candidates for the origin of the new $Q_A^{\bullet-}Fe^{2+}$ signal is the $Q_A^{\bullet-}Fe^{2+}Q_BH_2$ state. This would fit with formate inhibition of electron transfer being due to inhibition of Q_BH_2 release from the site [27,33]. In the most recent crystal structure Q_C is close to the Q_B site (~17 Å) and suggestions have been made for its role in electron transfer as a staging post for Q_BH_2 replacement [23]. If Q_C represents the one-quinone pool reported by Fufezan et al. [48], then it is possible that formate interferes with the exchange process with Q_C. This could occur as a long range influence from its binding to the iron or as a second binding effect closer Q_B and Q_C. It has already been suggested that a second bicarbonate/formate site other than the iron ligation site may be present [32]. This suggestion was mainly based on the observation that DCMU addition inhibited formate binding. Here we suggest it could interfere with Q_B/Q_C exchange. Further experimentation is required in order to address this idea.

If formate interferes with the protonation pathways as suggested earlier [24] and [34] then it is worth considering the two deprotonated forms of the state of $Q_A^{\bullet-}Fe^{2+}Q_BH_2$, that is to say $Q_A^{\bullet-}Fe^{2+}Q_BH^-$ and $Q_A^{\bullet-}Fe^{2+}Q_B^{\bullet-}$ states as a possible origin of the new EPR signal. While we do not rule out these options, in the absence of experimental arguments, the $Q_A^{\bullet-}Fe^{2+}Q_BH_2$ (formate) state is the more conservative assignment and this will be used in the remaining discussion.

Spectral simulations of all the semiquinone–iron signals demonstrate that the modified $Q_A^{\bullet-}Fe^{2+}Q_BH_2$ (formate) state is significantly different from all previously measured signals at around $g = 1.84$. The magnitude of the difference is significantly larger than that seen between different species or from the binding of herbicides to the Q_B pocket. Thus Q_BH_2 occupation of the Q_B pocket alone is unlikely to explain the "modified state" of the $Q_A^{\bullet-}Fe^{2+}$. Indeed from the range of semiquinone–iron signals present in the literature, the effects of point mutations and binding of herbicides and the nature of the spectral changes seen, it seems that significant changes in the spectrum of $Q_A^{\bullet-}Fe^{2+}$ reflect changes is the vicinity of the $Q_A^{\bullet-}$ or the Fe^{2+}. In our simulations, the zero-field splitting of the Fe^{2+} was different for the modified state. A similar change was seen for the simulations of the $g \sim 1.9$ signal [34] where an increase in the zero-field splitting was inferred of up to 7 K^{-1}. This was interpreted as being due to a change in the first coordination sphere of the iron, i.e. the CO_3^{2-} ligand significantly altered the Fe^{2+}. It is suggested that an analogous modification albeit of lesser magnitude, may occur for the new formate-modified $Q_A^{\bullet-}Fe^{2+}Q_BH_2$ state. Potentially the introduction of a charged group in the 1st/2nd coordination sphere of the iron could induce this effect. One possibility is that formate prevents the re-protonation of a protein residue (close to the iron) after Q_BH_2 formation. An alternative explanation along the same lines is that an additional formate ion is bound (or formed by deprotonation of formic acid) during Q_B reduction.

4.4. Formate-induced inhibition

The EPR study shows that formate inhibits the electron transfer after two electrons arrive on Q_B, as manifest by the formation of the $Q_A^{\bullet-}Fe^{2+}Q_BH_2$ (formate) state on the third flash. This fits with results reported earlier using fluorescence [30] and electronic absorption measurements [27]. In earlier work the $Q_A^{\bullet-}$ oxidation kinetic slowed by more than 2 orders of magnitude, from around 1 ms to 100–200 ms on the third flash [27,30]. Here however the $Q_A^{\bullet-}$ signal is still present in a sample frozen ~1 s second after a laser flash. Possible explanations for this difference include: (i) slower quinone exchange in the thermophile at room temperature (i.e. a species difference); and (ii) some centers lacking Q_C in the isolated PSII (i.e. a biochemical difference). Kinetic experiments on the present material measuring $Q_A^{\bullet-}$ decay by using fluorescence or optical absorption changes should resolve this issue.

Overall the data indicate that formate does not greatly modify electron transfer from $Q_A^{\bullet-}$ to Q_B or $Q_A^{\bullet-}$ to $Q_B^{\bullet-}$. We know from the literature that the kinetics is slowed by a factor of 5 and 10 respectively. Given that the uninhibited electron transfer rate ($t_{1/2}$ around 400 and 800 μs) [76] is much faster than the decay of $S_2/_3Q_A^{\bullet-}$ ($t_{1/2} = 1$ s), then this slowing of the rate has little effect on the yield of the final charge separated state. In contrast, on the 3rd flash electron transfer is more drastically affected: (i) $Q_A^{\bullet-}$ begins to get trapped under the conditions of the EPR experiment; (ii) the advance of the charge accumulation states of the water oxidizing complex (S states) becomes less efficient (probably because of the long time for Q_BH_2 exchange compared to the flash spacing); and (iii) a new state is detected by EPR which we suggest is the $Q_A^{\bullet-}Fe^{2+}$ in the presence of a double-reduced form of Q_B. The observation that the main effect of formate on electron transfer occurs on the third turnover, fits with earlier observations in the literature using fluorescence and absorption measurements [27,30]. However the current work indicates that the block occurs with reduced quinone in the Q_B site rather than with an empty site.

The signals reported and characterized here allow the previously elusive $Q_B^{\bullet-}Fe^{2+}$state and the newly discovered, formate-inhibited, $Q_A^{\bullet-}Fe^{2+}Q_BH_2$ state to be easily monitored using EPR. These signals should be useful in future studies aimed at understanding in more detail the nature of the electron transfer inhibition induced by formate and potential regulatory mechanisms involving bicarbonate/carbonate. Indeed the signals are probably distinct enough to be useful for studies in physiologically relevant biological material.

Acknowledgments

This work was supported by the EU/Energy Network project SOLAR-H2 (FP7 contract 212508). We thank Gernot Renger for providing the ANT2p. Arezki Sedoud is supported by the IRTELIS training program of the CEA. Lisa Kastner was funded in part by a grant from the DRI of the CEA. A. Boussac and A. Krieger-Liszkay are acknowledged for helpful discussions. We thank Wolfgang Lubitz for reading the manuscript and for helpful suggestions.

Appendix A. Supplementary data

Supplementary data to this article can be found online at doi:10.1016/j.bbabio.2010.10.019.

References

[1] B.A. Diner, G.T. Babcock, Structure, dynamics, and energy conversion efficiency in photosystem II, in: D.R. Ort, C.F. Yocum (Eds.), Oxygenic Photosynthesis: The Light Reactions, Kluwer Academic, Dordecht, The Netherlands, 1996, pp. 213–247.

[2] F. Rappaport, B.A. Diner, Primary photochemistry and energetics leading to the oxidation of the Mn_4Ca cluster and to the evolution of molecular oxygen in Photosystem II, Coord. Chem. Rev. 252 (2008) 259–272.

[3] V. Petrouleas, A.R. Crofts, The iron–quinone acceptor complex, in: T. Wydrzynski, K. Satoh (Eds.), Photosystem II. The light-driven water: plastoquinone oxidoreductase, Springer, Dordecht, The Netherlands, 2005, pp. 177–206.

[4] B. Bouges-Bouquet, Electron transfer between the two photosystems in spinach chloroplasts, Biochim. Biophys. Acta 314 (1973) 250–256.

[5] B.R. Velthuys, J. Amesz, Charge accumulation at reducing side of system 2 of photosynthesis, Biochim. Biophys. Acta 333 (1974) 85–94.

[6] B.R. Velthuys, Electron-dependent competition between plastoquinone and inhibitors for binding to Photosystem II, FEBS Lett. 126 (1981) 277–281.

[7] C.A. Wraight, Oxidation-reduction physical-chemistry of the acceptor quinone complex in bacterial photosynthetic reaction centers—evidence for a new model of herbicide activity, Isr. J. Chem. 21 (1981) 348–354.

[8] C.A. Wraight, Proton and electron transfer in the acceptor quinone complex of photosynthetic reaction centers from *Rhodobacter sphaeroides*, Front. Biosci. 9 (2004) 309–337.

[9] M.Y. Okamura, M.L. Paddock, M.S. Graige, G. Feher, Proton and electron transfer in bacterial reaction centers, Biochim. Biophys. Acta 1458 (2000) 148–163.

[10] A.W. Rutherford, How close is the analogy between the reaction center of PSII and that of purple bacteria? 2. The electron acceptor side, in: J. Biggins (Ed.), Progress in Photosynthesis Research, Martinus Nijhoff, Dordecht, The Netherlands, 1987, pp. 277–283.

[11] H. Michel, J. Deisenhofer, Relevance of the photosynthetic reaction center from purple bacteria to the structure of Photosystem-II, Biochemistry 27 (1988) 1–7.

[12] A.W. Rutherford, Photosystem-II, the water-splitting enzyme, Trends Biochem. Sci. 14 (1989) 227–232.

[13] A. Trebst, The topology of the plastoquinone and herbicide binding peptides of photosystem II in the thylakoid membrane, Z. Naturforsch. C 41 (1986) 240–245.

[14] R.J. Debus, B.A. Barry, G.T. Babcock, L. McIntosh, Site-directed mutagenesis identifies a tyrosine radical involved in the photosynthetic oxygen-evolving system, Proc. Natl Acad. Sci. USA 85 (1988) 427–430.

[15] W.F.J. Vermaas, A.W. Rutherford, O. Hansson, Site-directed mutagenesis in photosystem II of the *Cyanobacterium synechocystis sp* PCC6803—donor-D is a tyrosine residue in the D2-protein, Proc. Natl Acad. Sci. USA 85 (1988) 8477–8481.

[16] B. Svensson, I. Vass, E. Cedergren, S. Styring, Structure of donor side components in photosystem II predicted by computer modelling, EMBO J. 9 (1990) 2051–2059.

[17] R.T. Sayre, B. Andersson, L. Bogorad, The topology of a membrane protein: the orientation of the 32 kd Q_B-binding chloroplast thylakoid membrane protein, Cell 47 (1986) 601–608.

[18] O. Nanba, K. Satoh, Isolation of a photosystem II reaction center consisting of D-1 and D-2 polypeptides and cytochrome b-559, Proc. Natl Acad. Sci. USA 84 (1987) 109–112.

[19] P. Dorlet, A.W. Rutherford, S. Un, Orientation of the tyrosyl D, pheophytin anion, and semiquinone $Q_A^{\bullet -}$ radicals in photosystem II determined by high-field electron paramagnetic resonance, Biochemistry 39 (2000) 7826–7834.

[20] T. Yoshii, H. Hara, A. Kawamori, K. Akabori, M. Iwaki, S. Itoh, ESEEM study of the location of spin-polarized chlorophyll-quinone radical pair in membrane-oriented spinach photosystems I and II complexes, Appl. Magn. Reson. 16 (1999) 565–580.

[21] A. Zouni, H.T. Witt, J. Kern, P. Fromme, N. Krauss, W. Saenger, P. Orth, Crystal structure of photosystem II from *Synechococcus elongatus* at 3.8 angstrom resolution, Nature 409 (2001) 739–743.

[22] K.N. Ferreira, T.M. Iverson, K. Maghlaoui, J. Barber, S. Iwata, Architecture of the photosynthetic oxygen-evolving center, Science 303 (2004) 1831–1838.

[23] A. Guskov, J. Kern, A. Gabdulkhakov, M. Broser, A. Zouni, W. Saenger, Cyanobacterial photosystem II at 2.9-angstrom resolution and the role of quinones, lipids, channels and chloride, Nat. Struct. Mol. Biol. 16 (2009) 334–342.

[24] J.J.S. Van Rensen, W.J.M. Tonk, S.M. Debruijn, Involvement of bicarbonate in the protonation of the secondary quinone electron-acceptor of Photosystem II via the non-heme iron of the quinone–iron acceptor complex, FEBS Lett. 226 (1988) 347–351.

[25] R. Hienerwadel, C. Berthomieu, Bicarbonate binding to the non-heme iron of photosystem II investigated by fourier transform infrared difference spectroscopy and ^{13}C-labeled bicarbonate, Biochemistry 34 (1995) 16288–16297.

[26] P. Jursinic, J. Warden, Govindjee, Major site of bicarbonate effect in system-II reaction evidence from ESR signal-IIvf, fast fluorescence yield changes and delayed light-emission, Biochim. Biophys. Acta 440 (1976) 322–330.

[27] U. Siggel, R. Khanna, G. Renger, Govindjee, Investigation of the absorption changes of the plasto-quinone system in broken chloroplasts. The effect of bicarbonate-depletion, Biochim. Biophys. Acta 462 (1977) 196–207.

[28] H.H. Robinson, J.J. Eaton-Rye, J.J.S. van Rensen, Govindjee, The effects of bicarbonate depletion and formate incubation on the kinetics of oxidation-reduction reactions of the Photosystem II quinone acceptor complex, Z. Naturforsch. C 39 (1984) 382–385.

[29] J.J. Eaton-Rye, Govindjee, Electron-transfer through the quinone acceptor complex of Photosystem-II after one or 2 actinic flashes in bicarbonate-depleted spinach thylakoid membranes, Biochim. Biophys. Acta 935 (1988) 248–257.

[30] M.P.J. Pulles, Govindjee, R. Govindjee, H.J. van Gorkom, L.N.M. Duysens, Inhibition of reoxidation of secondary-electron acceptor of Photosystem-II by bicarbonate depletion, Biochim. Biophys. Acta 449 (1976) 602–605.

[31] J. Farineau, P. Mathis, Effect of bicarbonate on electron transfer between plastoquinones in Photosystem II, in: Y. Inoue, A.R. Crofts, Govindjee, N. Murata, G. Renger, K. Satoh (Eds.), The oxygen evolving system of photosynthesis, Academic Press, Inc., 1983, pp. 317–325.

[32] D.J. Blubaugh, Govindjee, The molecular mechanism of the bicarbonate effect at the plastoquinone reductase site of photosynthesis, Photosynth. Res. 19 (1988) 85–128.

[33] J.J.S. van Rensen, V.V. Klimov, Role of bicarbonate in Photosystem II, in: T.J. Wydrzynski, K. Satoh (Eds.), Advances in photosynthesis and respiration oxygenic photosynthesis: Photosystem II. The light driven water: Plastoquinone oxidoreductase, Springer, Dordrecht, 2005, pp. 329–346.

[34] N. Cox, L. Jin, A. Jaszewski, P.J. Smith, E. Krausz, A.W. Rutherford, R. Pace, The semiquinone–iron complex of photosystem II: Structural insights from ESR and theoretical simulation; evidence that the native ligand to the non-heme iron is carbonate, Biophys. J. 97 (2009) 2024–2033.

[35] J.H.A. Nugent, B.A. Diner, M.C.W. Evans, Direct detection of the electron-acceptor of photosystem-II - evidence that Q is an iron–quinone complex, FEBS Lett. 124 (1981) 241–244.

[36] A.W. Rutherford, P. Mathis, A relationship between the midpoint potential of the primary acceptor and low-temperature photochemistry in Photosystem II, FEBS Lett. 154 (1983) 328–334.

[37] A.W. Rutherford, J.L. Zimmermann, A new EPR signal attributed to the primary plastosemiquinone acceptor in Photosystem II, Biochim. Biophys. Acta 767 (1984) 168–175.

[38] W.F.J. Vermaas, A.W. Rutherford, Electron-paramagnetic-res measurements on the effects of bicarbonate and triazine resistance on the acceptor side of Photosystem II, FEBS Lett. 175 (1984) 243–248.

[39] J.L. Zimmermann, A.W. Rutherford, Photoreductant-induced oxidation of Fe^{2+} in the electron–acceptor complex of Photosystem II, Biochim. Biophys. Acta 851 (1986) 416–423.

[40] F. van Mieghem, K. Brettel, B. Hillmann, A. Kamlowski, A.W. Rutherford, E. Schlodder, Charge recombination reactions in Photosystem II.1. Yields, recombination pathways, and kinetics of the primary pair, Biochemistry 34 (1995) 4798–4813.

[41] F. Mamedov, M.M. Nowaczyk, A. Thapper, M. Rogner, S. Styring, Functional characterization of monomeric Photosystem II core preparations from *Thermosynechococcus elongatus* with or without the Psb27 protein, Biochemistry 46 (2007) 5542–5551.

[42] S. Demeter, C. Goussias, G. Bernat, L. Kovacs, V. Petrouleas, Participation of the $g=1.9$ and $g=1.82$ EPR forms of the semiquinone–iron complex $Q_A^{\cdot-}\cdot Fe^{2+}$ of photosystem II in the generation of the Q and C thermoluminescence bands, respectively, FEBS Lett. 336 (1993) 352–356.

[43] V. Petrouleas, Y. Deligiannakis, B.A. Diner, Binding of carboxylate anions at the non-heme Fe(II) of PS II. II. Competition with bicarbonate and effects on the Q_A/Q_B electron transfer rate, Biochim. Biophys. Acta 1188 (1994) 271–277.

[44] D.F. Ghanotakis, G.T. Babcock, C.F. Yocum, Structural and catalytic properties of the oxygen-evolving complex—correlation of polypeptide and manganese release with the behavior of Z+ in chloroplasts and a highly resolved preparation of the PSII complex, Biochim. Biophys. Acta 765 (1984) 388–398.

[45] A.W. Rutherford, J.L. Zimmermann, P. Mathis, EPR of PSII-interactions, herbicide effects and new signal, in: C. Sybesma (Ed.), Advances in Photosynthesis Research, Martinus Nijhoff, Junk, W., Dordecht, The Netherlands, 1984, pp. 445–448.

[46] B. Hallahan, S. Ruffle, S. Bowden, J.H.A. Nugent, Identification and characterization of EPR signals involving Q_B semiquinone in plant Photosystem II, Biochim. Biophys. Acta 1059 (1991) 181–188.

[47] A.R. Corrie, J.H.A. Nugent, M.C.W. Evans, Identification of EPR Signals from the States $Q_A^{\cdot-}Q_B^{-}$ and $Q_B^{\cdot-}$ in Photosystem-II from *Phormidium laminosum*, Biochim. Biophys. Acta 1057 (1991) 384–390.

[48] C. Fufezan, C.X. Zhang, A. Krieger-Liszkay, A.W. Rutherford, Secondary quinone in photosystem II of *Thermosynechococcus elongatus*: Semiquinone–iron EPR signals and temperature dependence of electron transfer, Biochemistry 44 (2005) 12780–12789.

[49] J. Kern, B. Loll, C. Luneberg, D. DiFiore, J. Biesiadka, K.D. Irrgang, A. Zouni, Purification, characterisation and crystallisation of photosystem II from *Thermosynechococcus elongatus* cultivated in a new type of photobioreactor, Biochim. Biophys. Acta 1706 (2005) 147–157.

[50] J. Kruk, K. Strzalka, Redox changes of cytochrome b_{559} in the presence of plastoquinones, J. Biol. Chem. 276 (2001) 86–91.

[51] O. Kaminskaya, V.A. Shuvalov, G. Renger, Evidence for a novel quinone-binding site in the photosystem II (PS II) complex that regulates the redox potential of cytochrome b559, Biochemistry 46 (2007) 1091–1105.

[52] U. Muhlenhoff, F. Chauvat, Gene transfer and manipulation in the thermophilic cyanobacterium *Synechococcus elongatus*, Mol. Gen. Genet. 252 (1996) 93–100.

[53] A. Boussac, F. Rappaport, P. Carrier, J.M. Verbavatz, R. Gobin, D. Kirilovsky, A.W. Rutherford, M. Sugiura, Biosynthetic Ca^{2+}/Sr^{2+} exchange in the photosystem II oxygen-evolving enzyme of *Thermosynechococcus elongatus*, J. Biol. Chem. 279 (2004) 22809–22819.

[54] M. Sugiura, Y. Inoue, Highly purified thermo-stable oxygen-evolving photosystem II core complex from the thermophilic cyanobacterium *Synechococcus elongatus* having his-tagged CP43, Plant Cell Physiol. 40 (1999) 1219–1231.

[55] J. Cao, Govindjee, Bicarbonate effect on electron flow in a cyanobacterium *Synechocystis* PCC 6803, Photosynth. Res. 19 (1988) 277–285.
[56] S. Stoll, A. Schweiger, EasySpin, a comprehensive software package for spectral simulation and analysis in EPR, J. Magn. Reson. 178 (2006) 42–55.
[57] I. Sinning, H. Michel, P. Mathis, A.W. Rutherford, Characterization of 4 herbicide-resistant mutants of *Rhodopseudomonas viridis* by genetic-analysis, electron-paramagnetic resonance, and optical spectroscopy, Biochemistry 28 (1989) 5544–5553.
[58] J.S. Leigh, P.L. Dutton, Primary electron acceptor in photosynthesis, Biochem. Biophys. Res. 46 (1972) 414-&.
[59] W.F. Butler, R. Calvo, D.R. Fredkin, R.A. Isaacson, M.Y. Okamura, G. Feher, The electronic-structure of Fe2+ in reaction centers from *Rhodopseudomonas sphaeroides*.3. Electron-paramagnetic-res measurements of the reduced acceptor complex, Biophys. J. 45 (1984) 947–973.
[60] J.H.A. Nugent, A.R. Corrie, C. Demetriou, M.C.W. Evans, C.J. Lockett, Bicarbonate binding and the properties of Photosystem II electron-acceptors, FEBS Lett. 235 (1988) 71–75.
[61] B.R. Velthuys, J.W.M. Visser, The reactivation of EPR signal II in chloroplasts treated with reduced dichlorophenol-indophenol: Evidence against a dark equilibrium between two oxidation states of the oxygen evolving system, FEBS Lett. 55 (1975) 109–112.
[62] A.W. Rutherford, A. Boussac, P. Faller, The stable tyrosyl radical in Photosystem II: why D? Biochim. Biophys. Acta 1655 (2004) 222–230.
[63] G.C. Dismukes, Y. Siderer, Intermediates of a polynuclear manganese center involved in photosynthetic oxidation of water, Proc. Natl Acad. Sci. USA 78 (1981) 274–278.
[64] G.W. Brudvig, J.L. Casey, K. Sauer, The effect of temperature on the formation and decay of the multiline electron-paramagnetic-res signal species associated with photosynthetic oxygen evolution, Biochim. Biophys. Acta 723 (1983) 366–371.
[65] Y.M. Feyziev, D. Yoneda, T. Yoshii, N. Katsuta, A. Kawamori, Y. Watanabe, Formate-induced inhibition of the water-oxidizing complex of photosystem II studied by EPR, Biochemistry 39 (2000) 3848–3855.
[66] A. Jajoo, N. Katsuta, A. Kawamori, An EPR study of the pH dependence of formate effects on Photosystem II, Plant Physiol. Biochem. 44 (2006) 186–192.
[67] N. Cox, F.M. Ho, N. Pewnim, R. Steffen, P.J. Smith, K.G.V. Havelius, J.L. Hughes, L. Debono, S. Styring, E. Krausz, R.J. Pace, The S-1 split signal of photosystem II; a tyrosine-manganese coupled interaction, Biochim. Biophys. Acta 1787 (2009) 882–889.
[68] J.L. Hughes, A.W. Rutherford, M. Sugiura, E. Krausz, Quantum efficiency distributions of photo-induced side-pathway donor oxidation at cryogenic temperature in photosystem II, Photosynth. Res. 98 (2008) 199–206.
[69] C.A. Wraight, Iron–quinone interactions in electron-acceptor region of bacterial photosynthetic reaction centers, FEBS Lett. 93 (1978) 283–288.
[70] A.W. Rutherford, M.C.W. Evans, High-potential semiquinone–iron signal in *Rhodopseudomonas viridis* is the specific quinone secondary-electron acceptor in the photosynthetic reaction center, FEBS Lett. 104 (1979) 227–230.
[71] P. Faller, C. Fufezan, A.W. Rutherford, Side-path electrondonnors: cytochrome b559, chlorophyll Z and beta-caroten, in: T.J. Wydrzynski, K. Satoh (Eds.), Photosystem II: The Light-Driven water: Plastoquinone Oxidoreductase, Springer, Dordecht, the Netherlands, 2005, pp. 347–365.
[72] A.W. Rutherford, M.C.W. Evans, High-potential semiquinone–iron type epr signal in *Rhodopseudomonas viridis*, FEBS Lett. 100 (1979) 305–308.
[73] G.N. Johnson, A. Boussac, A.W. Rutherford, The origin of 40-50 °C thermoluminescence bands in Photosystem II, Biochim. Biophys. Acta 1184 (1994) 85–92.
[74] A.W. Rutherford, J.L. Zimmermann, P. Mathis, The effect of herbicides on components of the PSII reaction center measured by electron-paramagnetic-res, FEBS Lett. 165 (1984) 156–162.
[75] J.J.S. van Rensen, C.H. Xu, Govindjee, Role of bicarbonate in photosystem II, the water-plastoquinone oxido-reductase of plant photosynthesis, Physiol. Plant. 105 (1999) 585–592.
[76] R. de Wijn, H.J. van Gorkom, Kinetics of electron transfer from Q_A to Q_B in photosystem II, Biochemistry 40 (2001) 11912–11922.